ALICE Highlights

Ionut Cristian Arsene[1,2] for the ALICE Collaboration

[1]University of Oslo
[2]iarsene@cern.ch

Abstract. A summary including highlights of recent ALICE results, the status of the data taking in LHC Run 3 and of the ALICE detector upgrades is shown. The physics results are obtained mainly using the data recorded in pp, p–Pb and Pb–Pb during the LHC Run 2, but a set of results obtained in pp collisions with the Run 3 data is also discussed.

1 Introduction

ALICE, the dedicated experiment for relativistic heavy-ion physics at the Large Hadron Collider (LHC), had its major upgrades installed during the Long Shutdown 2 (2019-2021) and restarted data taking since the beginning of the LHC Run 3 in 2022. The upgrades allow for an approximately 50 times increase in readout rate, 3 to 6 times improvement in pointing resolution and secondary vertexing for forward muons [1]. The main upgraded detector subsystems are the Time Projection Chamber (TPC) [2] and the Inner Tracking System (ITS) [3]. In addition, ALICE installed two new subdetectors, the Muon Forward Tracker (MFT) [4] which allows the reconstruction of secondary vertices from beauty-hadron decays in the acceptance of the ALICE MUON arm, and the Fast Interaction Trigger (FIT) [5] which provides collision time and other global event characteristics such as collision multiplicity and event plane orientation. At the same time, ALICE upgraded its entire Online and Offline software framework (the O^2 project), and added the First Level Processors (FLP) and the Event Processor Node (EPN) computing nodes in order to cope with the much higher data throughput during the data taking. In Run 3 and 4, these upgrades will enable ALICE to record an integrated luminosity which is about 100 times larger in Pb–Pb and about 1000 times larger in pp and p–Pb collisions compared to the one recorded during the Run 1 and 2 with the barrel detectors.

The ALICE Collaboration recently published a comprehensive review [6] on the progress of the understanding of the high-density deconfined QCD matter produced at LHC energies by aggregating the results obtained so far with the Run 1 and 2 data. The highlights presented here will cover newer results obtained using either the Run 1 and 2 or the fresh Run 3 data and are grouped into a few categories: initial state (section 2), soft probes (section 3), hard and electromagnetic probes (section 4) and future upgrades (section 5). Detailed results were presented at this conference by ALICE in 30 parallel talks and their respective proceedings and 60 posters.

2 Initial state

ALICE presented several new results sensitive to the initial state of heavy-ion collisions, including measurements of high-p_{T} direct photons in Pb–Pb collisions, coherent and incoherent J/ψ production in ultra-peripheral Pb–Pb collisions (UPC), strangeness enhancement and collective-like behaviour in high-activity pp and p–Pb collisions.

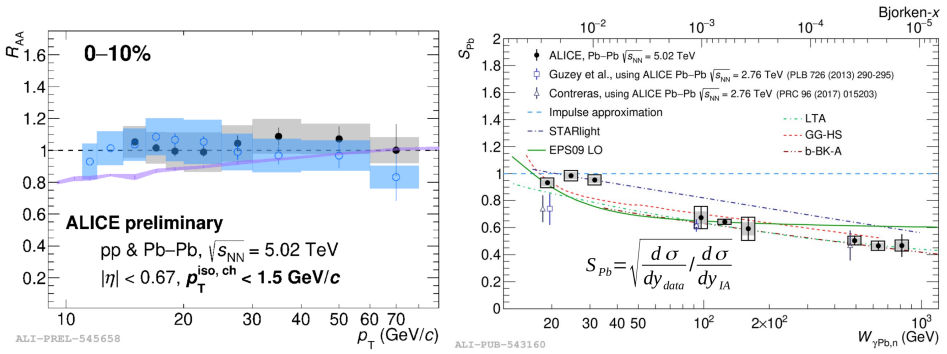

Figure 1. Left: High-p_{T} isolated photon R_{AA} as a function of p_{T} in 0-10% central Pb–Pb collisions. Right: Nuclear suppression factor for coherent J/ψ in Pb–Pb UPC collisions as a function of the photo-nuclear collision energy [8].

Direct photons with high-p_{T} are produced mainly in hard Compton and annihilation processes taking place in the first stages of the collision and escape the fireball without additional rescatterings. Their total production cross section is an important control probe for the initial state of the collision, while their event by event energy measurement provides the initial energy scale for the recoil jet in-medium modification measurements. The nuclear modification factor R_{AA} as a function of p_{T} for direct photons in the 10% most central Pb–Pb collisions is shown in the left panel of figure 1 and described in more details in Ref. [7]. The filled and open symbols correspond to the analysis being done with an isolation cone with a radius $R = \sqrt{(\Delta\eta^2 + \Delta\varphi^2)}$ of 0.2 and 0.4, respectively. The values of the R_{AA} are compatible with unity over the entire p_{T} interval presented, indicating that the photon yields are proportional to the number of binary collisions. The measurements are also compared to a JETPHOX NLO pQCD calculation (magenta band) using the nuclear modified PDFs nNNPDF30.

The cross section of coherently photoproduced J/ψ in Pb–Pb UPC collisions is sensitive to the gluon distributions in the nucleus. The recent ALICE measurement of the coherent photoproduction in UPC events are done in neutron emission event classes [8]. This helps narrowing down the relevant impact parameter range in the calculation of the photon flux, and provides a tag for the target and emitter nuclei. The new measurements done at $\sqrt{s_{\mathrm{NN}}}$ = 5.02 TeV extend the coverage in the photon-nucleus centre-of-mass energy up to 920 GeV [8, 9] corresponding to a Bjorken-x of $\approx 10^{-5}$. In the right panel of figure 1, the nuclear suppression factor computed based on the cross section measurements relative to the impulse approximation estimation, is shown as a function of the centre-of-mass energy. This ratio exhibits a decreasing trend towards high energy or low Bjorken-x, indicating an increasing degree of gluon suppression, compatible qualitatively with model calculations.

3 Soft probes

Several results on the soft probes or bulk properties of pp, p–Pb and Pb–Pb collisions were presented, including new Run 3 results in pp collisions on charged particle multiplicity, $\Omega^{\pm}$ baryons, (anti)(hyper)nuclei and proton-proton femtoscopy, and Run 2 data based results on strange particle yields, event-by-event fluctuations of net strange particles and net protons, correlations of event-by-event fluctuations of net-kaons and net-Ξ, and 3-body femtoscopy with 3 protons and with the proton-deuteron system.

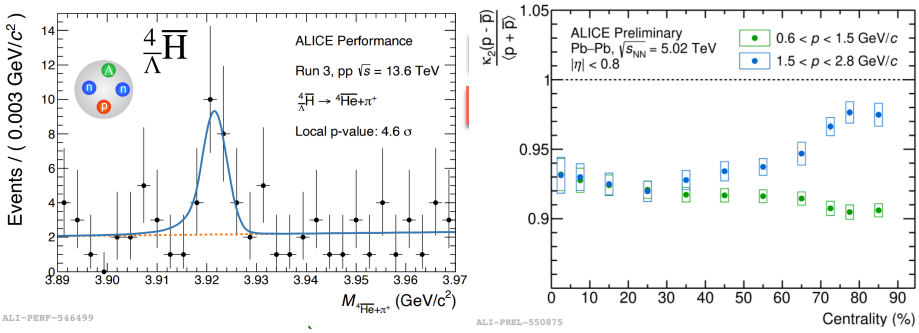

Figure 2. Left: Invariant mass distribution of $^{4}\overline{\mathrm{He}}$ and π^{+} pairs in pp collisions at $\sqrt{s}$ = 13.6 TeV. Right: Net-proton fluctuations as a function of centrality in two momentum intervals in Pb–Pb collisions at $\sqrt{s_{\mathrm{NN}}}$ = 5.02 TeV.

In the left panel of figure 2, the invariant mass distribution of identified $^{4}\overline{\mathrm{He}}$ and π^{+} pairs is shown, which exhibits a signal compatible with the $^{4}_{\Lambda}\overline{\mathrm{H}}$ state with a significance of 4.6σ. This result is obtained in pp collisions at $\sqrt{s}$ = 13.6 TeV using Run 3 data and is discussed in more details in Ref. [10]. The right hand-side panel of figure 2 shows the centrality dependence of the second order cumulant of the distribution of net-proton number κ_2 normalized to the average of the sum of proton and anti-proton yields. Values different than one indicate deviations from the Skellam baseline and Hadron Resonance Gas Model within the Grand Canonical Ensemble. The recent ALICE measurements in Pb–Pb collisions at $\sqrt{s_{\mathrm{NN}}}$ = 5.02 TeV exhibit values lower than one which may arise from local baryon number conservation. These new results extend the measurements to higher proton momentum (1.5 < p < 2.8 GeV/c) than existing measurements. The higher momentum protons exhibit a growing κ_2 towards peripheral collisions consistent with lattice QCD expectations [11] including magnetic field effects.

The left panel of figure 3 shows the correlation factor, ρ, of the event-by-event fluctuations of net-Ξ ($\Xi^{+} - \Xi^{-}$) and net-K ($\mathrm{K}^{+} - \mathrm{K}^{-}$) as a function of the charged-particle pseudorapidity density measured at midrapidity in pp, p–Pb and Pb–Pb collisions at $\sqrt{s_{\mathrm{NN}}}$ = 5.02 TeV [12]. The results show a clear anti-correlation of the net-Ξ and net-K which can be explained by the anti-correlation introduced by the strangeness conservation. However, the surviving anti-correlation up to the most central Pb–Pb collisions indicates that the strangeness conservation leads to a very large correlation length. In the right panel of figure 3, the femtoscopic proton-deuteron correlation function is shown for high-multiplicity pp collisions at $\sqrt{s}$ = 13 TeV [13]. The results are compared to a few model calculations and the best fit of the data is obtained with a source which models the proton-deuteron system as a 3-body system [14].

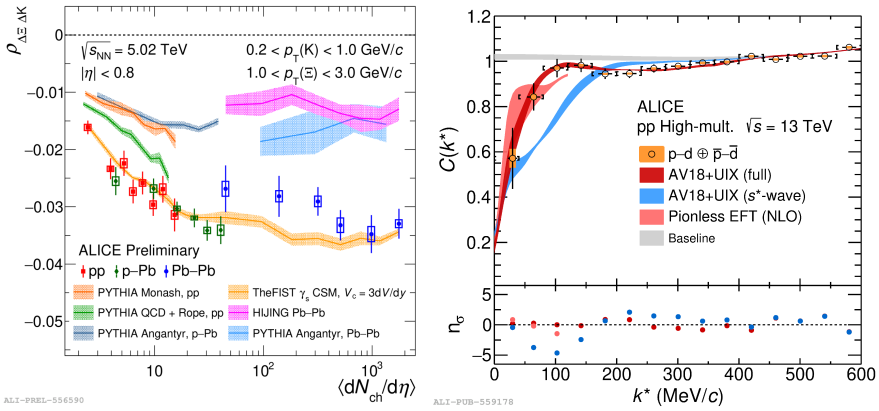

Figure 3. Left: Correlation strength of the net-Ξ and net-K fluctuation as a function of the event charged-particle multiplicity in pp, p–Pb and Pb–Pb collisions at $\sqrt{s_{NN}} = 5.02$ TeV. Right: Femtoscopic correlation function for the proton-deuteron system compared to different source models [14].

4 Hard and electromagnetic probes

Several ALICE measurements on hard and electromagnetic probes were discussed, including virtual direct photon measurements, open heavy-flavour and quarkonia, and jet substructure, suppression and broadening in Pb–Pb collisions with respect to pp collisions.

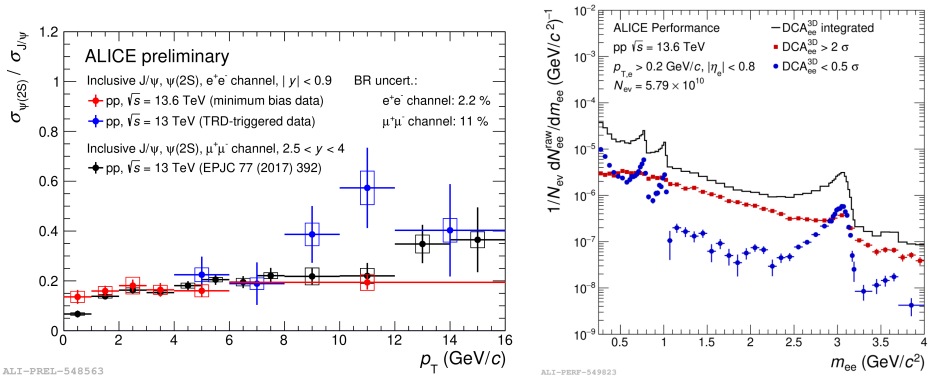

Figure 4. Left: $\psi(2S)/J/\psi$ ratio as a function of p_T in pp collisions at midrapidity in $\sqrt{s} = 13.6$ and 13 TeV and at forward rapidity in pp collisions at $\sqrt{s} = 13$ TeV. Right: Invariant mass distribution of electron-positron pairs before and after pair DCA selection in pp collisions at $\sqrt{s} = 13.6$ TeV.

The first charmonium measurements using Run 3 data were presented and discussed in detail in Ref. [15]. The measurement of the cross section ratio of $\psi(2S)$ to J/ψ as a function of p_T in pp collisions at $\sqrt{s} = 13.6$ TeV is shown in the left panel of figure 4. The results are compared to older results reported by ALICE at forward rapidity and to new results based on a Run 2 data sample triggered using the Transition Radiation Detector. In the right panel of figure 4, the invariant mass distribution of e^+e^- pairs obtained in pp collisions at $\sqrt{s} = 13.6$ TeV is shown [16]. The black distribution includes all the pairs, while the blue and the red data points represent distributions for prompt and non-prompt (displaced) e^+e^-

pairs, respectively, selected using the pair Distance-of-Closest-Approach (DCA) to the primary vertex. This selection allows the removal of background e^+e^- pairs from semi-leptonic beauty-hadron decays and is particularly efficient in Run 3 due to the upgraded ITS detector.

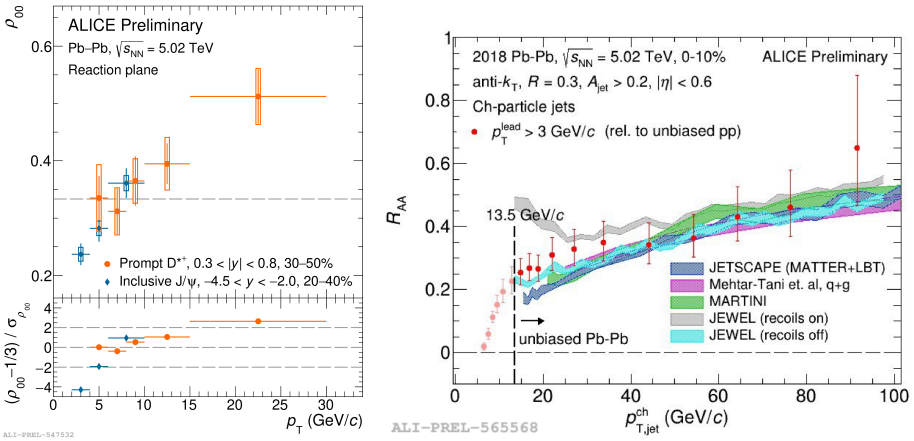

Figure 5. Left: D^{*+} and J/ψ spin alignment with respect to the event plane in Pb–Pb collisions at $\sqrt{s_{NN}}$ = 5.02 TeV. Right: Charged-jet R_{AA} as a function of jet p_T in 0-10% central Pb–Pb collisions, compared to model calculations.

ALICE also highlighted the first measurement of the spin alignment of the D^{*+} meson with respect to the reaction plane in Pb–Pb collisions at $\sqrt{s_{NN}}$ = 5.02 TeV [17]. These measurements (left panel of figure 5) show a hint of alignment at $p_T > 10$ GeV/c, but with an opposite sign compared to the alignment measured for $p_T < 6$ GeV/c for the J/ψ and light vector-mesons. Theory calculations are still missing. The charged-jet R_{AA} measured in the 10% most central Pb–Pb collisions at $\sqrt{s_{NN}}$ = 5.02 TeV was also discussed (right panel of figure 5) in the context of new analysis developments involving the usage of an event mixing technique for subtracting the jet background [18]. These results extend the measurement range down to p_T = 13.5 GeV/c and show a reasonable agreement with model calculations.

5 ALICE future upgrades

The status of the ALICE upgrade projects foreseen to be installed during the LHC Long Shut Down 3 and of the ALICE3, planned to replace ALICE in Run 5 and 6, were also presented. Figure 6 shows examples of the projected physics performance for the Forward Calorimeter (FoCal) and the ITS3 sub-detectors in the left and the right panels, respectively. The FoCal is an electromagnetic and hadronic calorimeter covering the acceptance $3.2 < \eta < 5.8$ with the main physics motivation of studying the non-linear QCD evolution at small Bjorken-x [19]. The main observables include isolated direct photons (see figure 6), neutral mesons, jets, heavy-quarkonia and correlations. The ITS3 project aims at replacing the innermost 3 pixel layers of the current ITS with truly cylindrical layers obtained by bending updated versions of the MAPS sensors which are thinner and are stitched together in 30 cm wafers. Such an upgrade will give an improvement of the pointing resolution by a factor 2 compared to the current ITS and enable high precision measurements of charm and multi-charm baryons [20] (see figure 6). The current status of the ALICE3 project, for which the research and development and the specific choices for the detector setup are in full swing, was presented and reported in more details in Ref. [20].

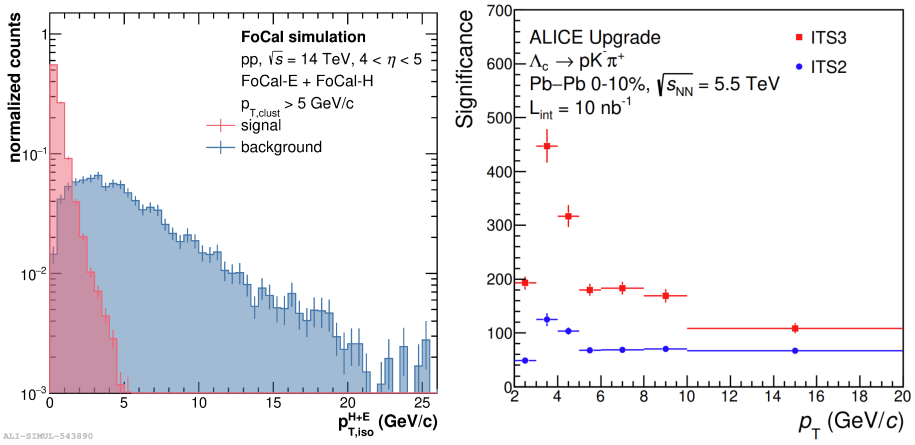

Figure 6. Left: Distribution of p_T in the isolation cone for signal and background photons simulated with the ALICE FoCal upgrade setup in pp collisions at $\sqrt{s}$ = 14 TeV. Right: Projected significance for the Λ_c measurement as a function of p_T in 0-10% central Pb–Pb collisions at $\sqrt{s_{NN}}$ = 5.5 TeV using the ALICE ITS3 upgrade.

6 Summary

We presented the structure of the ALICE highlights talk, a few selected physics results from both the old Run 1 and 2 data and the new Run 3 data, and we discussed the upcoming LS3 upgrade projects and the ALICE3 project meant to replace ALICE in Run 5 and 6.

References

[1] ALICE Collaboration, CERN-EP-2023-009 (2023)
[2] ALICE TPC Collaboration, JINST **16**, P03022 (2021)
[3] ALICE Collaboration, Nucl. Instrum. Meth. A **1032**, 166632 (2022)
[4] ALICE MFT Collaboration, OPEN-PHO-EXP-2020-004 (2020)
[5] ALICE Collaboration, Nucl. Instrum. Meth. A **1039**, 167021 (2022)
[6] ALICE Collaboration, CERN-EP-2022-227 (2022)
[7] Carolina Arata for the ALICE Collaboration, *these proceedings*
[8] ALICE Collaboration, JHEP **10**, 119 (2023)
[9] Simone Ragoni for the ALICE Collaboration, *these proceedings*
[10] Ivan Vorobyev for the ALICE Collaboration, *these proceedings*
[11] Ding Heng-Tong *et al.*, arXiv:2208.07285 [hep-lat]
[12] Mario Ciacco for the ALICE Collaboration, *these proceedings*
[13] Bhawani Singh for the ALICE Collaboration, *these proceedings*
[14] ALICE Collaboration, arXiv:2308.16120 [nucl-ex]
[15] Xiaozhi Bai for the ALICE Collaboration, *these proceedings*
[16] Daiki Sekihata for the ALICE Collaboration, *these proceedings*
[17] Luca Micheletti for the ALICE Collaboration, *these proceedings*
[18] Nadine Gruenwald for the ALICE Collaboration, *these proceedings*
[19] Florian Jonas for the ALICE Collaboration, *these proceedings*
[20] Isabella Sanna for the ALICE Collaboration, *these proceedings*